DOI: 10.26599/FSHW.2026.9251118

Contents lists available at SciOpen

Food Science and Human Wellness

journal homepage: https://www.sciopen.com/journal/2097-0765

China Food Publishing Co.

Characterization and antioxidant mechanisms of cherry-tomato derived exosome-like nanoparticles: Physicochemical properties, biomolecular cargo, and bioactivity

Ao Qu[1], Yuying Tang[1], Wenjing Liang[1], Runyan Wang[1], Pei Zhao[1], Shuaishuai Gao[1], Wen Zhang[1, 2, *], Zijian Wu[1, 2, 3, *]

[1] *Tianjin Key Laboratory of Food Science and Biotechnology, School of Biotechnology and Food Science, Tianjin University of Commerce, Tianjin 300134, China.*

[2] *Key Lab of Agricultural Products Low Carbon Cold Chain, Ministry of Agriculture and Rural Affairs, Tianjin 300134, China.*

[3] *Tianjin Key Laboratory of Edible Probiotics, Tianjin, 300134, China.*

ABSTRACT: Edible plant derived exosome-like nanoparticles (ELNs) have been shown to possess numerous bioactive properties with potential health benefits. Cherry tomatoes contain a wide variety of bioactive substances, however, cherry-tomato derived exosome-like nanoparticles (CTELNs) remain unexplored. This study employed a polyethylene glycol (PEG) precipitation method for the efficient isolation of CTELNs, evaluating five PEG concentrations (ranging from 10% to 30%, *w*/*v*) to determine the optimal precipitation conditions. Characterization and compositional analysis demonstrated that CTELNs isolated using 20% PEG displayed superior physicochemical properties. The small RNA sequencing analysis revealed a distinct enrichment of specific microRNAs (miRNA) implicated in the regulation of oxidative stress in CTELNs, such as miR156e-3p, miR156e-5p, miR390a-5p and miR9474-5p. Target gene prediction indicated that CTELNs potentially regulated pathways related to binding and catalytic activity. Notably, nine miRNAs were predicted to target the genes related to oxidative stress. *In vitro* cellular assays conducted on RAW264.7 cells showed that CTELNs exhibited no significant toxicity. Furthermore, functional validation further confirmed that CTELNs ameliorated H_2O_2-induced oxidative stress. The results of this work suggest that PEG precipitation for CTELNs isolation is feasible and the optimal PEG concentration is determined, which facilitates further exploration of edible plant derived exosome-like nanoparticles. Moreover, the remarkable antioxidant properties of CTELNs support their potential application as natural antioxidative agents in functional foods or nutraceuticals.

Keywords: Cherry tomato; Exosome-like nanoparticles; Polyethylene glycol precipitation; miRNA; Antioxidant ability

1. Introduction

Exosome-like nanoparticles (ELNs), a subset of extracellular vesicles (EVs), have attracted increasing research interest in recent years owing to their distinctive biological properties and broad application prospects [1]. In recent decades, plant-derived exosome-like nanoparticles (PELNs) isolated from edible

***Corresponding author**
wzjian@tjcu.edu.cn (Z.-J.W.) or wenzhang@tjcu.edu.cn (W.Z.).

Received 5 December 2025
Received in revised from 19 December 2025
Accepted 1 April 2026

plants, including lemon [2], ginger [3], grape [4], and tomato [5], have garnered significant research attention due to their inherent bioactive properties. Cherry tomato (*Solanum lycopersicum L. var. cerasiforme*), belonging to the same species as tomato, is rich in health-promoting compounds including polyphenols and lycopene[6], and has antioxidant, anticancer, immune-enhancing, and anti-aging properties [7]. Although the health benefits of cherry tomatoes have been discovered, research specifically on cherry-tomato derived exosome-like nanoparticles (CTELNs), particularly concerning their antioxidant molecular composition and mechanism of action, remains largely unexplored. The characteristics and biological activity of CTELNs remain entirely unexplored, representing a significant knowledge gap.

PELNs contain functional biomolecules, such as proteins, lipids, and nucleic acids, which play a fundamental part in facilitating intercellular communication [8]. Among the cargos of PELNs, microRNAs (miRNAs) are key regulators of gene expression that modulate a wide array of functional pathways, which has garnered significant research interest [9]. There is growing evidence that natural nanoparticles have therapeutic potential to alleviate oxidative stress-related conditions. Camel milk-derived exosomes exert potent cytoprotective effects by upregulating superoxide dismutase (SOD) activity [10]. Human umbilical cord mesenchymal stem cells (MSCs)-derived exosomes facilitate hepatic oxidative damage repair through targeted delivery of glutathione peroxidase (GSH-Px) 1 [11]. Ginger-derived extracellular nanoparticles exhibit significant hepatoprotection against ethanol-induced liver injury in murine models by attenuating oxidative stress [12]. Together, these findings emphasize the specific advantages of natural nanoparticles in combating oxidative damage in different tissues. Although these advantages highlight the functional potential of natural nanoparticles, the specific miRNA repertoire responsible for mediating their antioxidant effects remains largely uncharacterized. With the advancement of omics technologies, miRNA sequencing has emerged as a powerful tool for comprehensively profiling miRNA contents within nanoparticles, providing critical insights into their mechanism of action. For instance, miR166g, miR168b-5p, miR396a-5p, miR159b-3p, and miR159a in strawberry-derived extracellular vesicle-like nanoparticles have been found to be implicated in conferring antioxidant properties [13]. miR396b-5p, miR166b-3p, miR162a-3p, and miR159a have been reported to possess cross-regulatory functions in modulating oxidative stress responses within human cells [14]. Thus, in the study, miRNA sequencing was employed to systematically characterize the miRNA profile of CTELNs, aiming to identify antioxidant activity-related miRNAs that may underlie their cytoprotective function.

Currently, the reported methods for the isolation of PELNs include ultracentrifugation (UC), ultrafiltration, polyethylene glycol (PEG) precipitation [15], size exclusion chromatography (SEC) [8], and microfluidic techniques [12]. Among them, UC represents a fundamental technique for exosome isolation and is known as the “gold method” for the isolation. This method relies on the principle that exosomes, being denser and smaller than other cellular components, sediment at higher centrifugal force. Despite its widespread use, UC requires careful optimization of parameters, such as rotor type, centrifugation time and speed, to ensure high yield and purity while minimizing vesicle aggregation or damage [16]. Recently, the

isolation of PELNs has been achieved using a PEG precipitation approach, although this method was originally intended for virus isolation. This scientific reason arises from the comparable biophysical characteristics exhibited by both viruses and PELNs [17]. Importantly, recent advancements have revealed that tomato-derived EVs isolated through PEG precipitation are an environmentally friendly and cost-effective drug delivery system [18]. PEG molecules, due to their hydrophilic and polymeric nature, compete with exosomes for solvation in the aqueous phase. This competition reduces the solubility of exosomes, leading to their aggregation and subsequent precipitation. During this incubation, exosomes are forced out of solution and form a pellet upon centrifugation [19]. Therefore, a PEG precipitation method enables simultaneous isolation and purification of exosomes while maintaining satisfactory yield and purity comparable to the more expensive UC method. The method demonstrates significant utility as a cost-effective and efficient alternative to specialized equipment and commercial exosome isolation kits.

This study aimed to isolate and characterize CTELNs using the PEG precipitation method. The CTELNs were comprehensively characterized, including particle size, zeta potential, and transmission electron microscopy (TEM). In addition, protein and RNA content analyses were performed. To gain deeper insight into the molecular composition, miRNA sequencing was carried out to reveal a significant enrichment of specific miRNAs within CTELNs that are functionally associated with oxidative stress responses. Furthermore, functional investigations confirmed that CTELNs effectively mitigated H_2O_2-induced oxidative stress in RAW264.7 cells. This study highlights the potential of CTELNs as a novel natural antioxidant agent, and provides a foundation for future exploration into their therapeutic applications in oxidative stress-related diseases.

2. Materials and methods

2.1 Materials

The “Qianxi” cherry tomatoes at the ripe stage (fully red-colored) were purchased from a local supermarket (Tianjin, China). The fruits were stored in a refrigerated container at 4 ℃. PEG 8000 was purchased from Sigma (China). The BCA protein assay kit, LDH cytotoxicity assay kit, and PKH67 exosome labeling kit were from Beyotime Biotechnology (Shanghai, China). Trizol was from Thermo Fisher Scientific. cDNA synthesis kit, miRNA universal qPCR SYBR master mix, cDNA synthesis super mix, and universal blue qPCR SYBR green master mix were from Yeasen Biotechnology Co., Ltd. (Shanghai, China). Dulbecco’s Modified Eagle Medium (DMEM) was from Gibco (China). Fetal bovine serum (FBS) and penicillin-streptomycin were from Heyuan Liji Biotechnology Co., Ltd. (Shanghai, China). CCK-8 was from Solarbio (Beijing, China). Assay kits for SOD, GSH-Px and malondialdehyde (MDA) were from Nanjing Jiancheng Bioengineering Institute (Nanjing, China).

2.2 Isolation of CTELNs

CTELNs were isolated by PEG precipitation [15], with minor modifications. Briefly, the fruits were weighed in proportion to 100 mL PBS, crushed and the juice was collected. Supernatants were collected by

3 steps of centrifugation at 4 ℃ (1,000×g for 10 min, 3,000×g for 30 min, and 10,000×g for 30 min). The obtained supernatant was subjected to ultrafiltration through a 10,000 MWCO membrane by centrifugation at 3,500×g for 30 min. Concentrated juice was then filtered using a 0.45 μm membrane. The supernatants were mixed with an equal volume of PEG 8000 solutions at varying concentrations (10%, 12%, 16%, 20%, 30%, *w*/*v*) and incubated overnight. The next day, CTELNs were concentrated by centrifugation at 10,000×g for 30 min. The supernatants were discarded and the pellets were resuspended in PBS. All the steps were conducted at 4 ℃.

2.3 Particle size, particle concentration, and zeta potential

The particle size, particle concentration, and zeta potential of the CTELNs were determined by nanoparticle tracking analysis (NTA) (NS300, UK) and Zeta-sizer Nano instrument (Malvern, UK) at 25 °C based on a recent study [17]. Each test was replicated 3 times.

2.4 TEM

The morphological structure was characterized using a previous approach [20]. Briefly, the samples were deposited onto a copper grid for 5 min. Subsequently, 1% phosphotungstic acid was applied for negative staining for 2 min. Samples underwent a drying process and were subsequently visualized using an electron microscope. The micrographs were captured with a LaB6 (Tecnai G2 Spirit TWIN, FEI).

2.5 Total protein analysis

2.5.1 Total protein extraction

To extract the total protein from CTELNs, RIPA lysis buffer was used in the experimental procedure [21]. CTELNs were lysed by adding 200 μL strong lysis buffer and were agitated on ice for 30 min. The supernatant was collected by centrifugation at 12,000 rpm for 15 min.

2.5.2 Total protein content

The total protein content in the CTELNs was determined by employing the BCA protein assay kit following the manufacturer's instructions. Briefly, to prepare the BCA working solution, reagent A was mixed with reagent B in a ratio of 50:1. CTELNs suspension was then mixed with 200 μL BCA working solution, and the mixture was incubated at 37 °C for 30 min. The absorption was then quantified using a microplate reader (Infinite M200 pro NanoQuant) at a wavelength of 562 nm. Each sample was tested in triplicate to ensure accuracy.

2.5.3 Sodium dodecyl sulfate-polyacrylamide gel electrophoresis (SDS-PAGE)

The protein of CTELNs were separated by SDS-PAGE on a 10% gel. The gel underwent staining with Coomassie Brilliant Blue R250 and was subsequently rinsed using a destaining solution until the background attained a clear state.

2.6 Total RNA analysis

2.6.1 Total RNA extraction

The total RNA from CTELNs was extracted using the Trizol method [18]. Briefly, Trizol reagent was added to the CTELNs, followed by the addition of chloroform. Then, the aqueous phase was collected by centrifuging the mixture at 12,000 rpm, 4 ℃ for 15 min. Isopropanol was added to the aqueous phase and kept at -20 ℃ overnight to facilitate RNA precipitation. The next day, after centrifugation at 12,000 rpm, 4 ℃ for 30 min, the precipitation was washed with 70% ethanol solution and centrifuged again at 12,000 rpm, 4 ℃ for 2 min. The RNA was finally dissolved in RNase-free water. The purity was determined using a NanoPhotometer spectrophotometer. Each test was replicated 3 times.

2.6.2 Agarose gel electrophoresis

After RNA extraction, the degradation and contamination of RNA were verified using 1% agarose gels. After the sample was loaded, the electrophoresis time was approximately 30 min, and after the electrophoresis, the gel was removed and placed in a gel imager (Tanon 1600) to irradiate the gel.

2.7 MiRNA sequencing of CTELNs

Small RNAs were reversely transcribed, enriched to generate a cDNA library and sequenced on a DNBSEQ platform. The clean tags were sequentially aligned with miRNA to the tomato reference genome using Bowtie2 (Version 2.2.5). The target genes of miRNAs were predicted by Tapir (Version 1.2) and TargetFinder (Version 1.0). Target gene functional enrichment analysis proceeded with the Gene Ontology (GO) and Kyoto Encyclopedia of Genes and Genomes (KEGG) annotation.

2.8 Quantitative real-time polymerase chain reaction (qRT-PCR)

To validate sequencing and computational results, six miRNAs were selected for qRT-PCR validation. The GAPDH gene served as the internal control, and specific primers were designed based on cDNA sequences (Table S1-S2). qRT-PCR was performed on a Bio-Rad CFX96 Real-Time system. Relative gene expression levels were calculated using the Livak and Schmittgen $2^{-\Delta\Delta Ct}$ method [22]. Each sample underwent triplicate PCR amplification.

2.9 Cell viability

RAW264.7 cells were cultured in DMEM with 10% (*v*/*v*) FBS and 1% (*v*/*v*) penicillin-streptomycin. The cells were incubated at 37 ℃ with 5% CO_2. The cells were split at a ratio of 1:3 at 80% confluence and were not maintained beyond passage 20. A cell viability assay was carried out in accordance with a previously published protocol [23], with slight modifications. The impact of CTELNs on RAW264.7 cells viability was assessed using the CCK-8 assay, and the content of lactate dehydrogenase (LDH) was determined in accordance with the manufacturer's instructions. Each test was replicated 3 times.

2.10 Cellular uptake assay

CTELNs were labeled with PKH67 according to the manufacturer's instructions [24]. Briefly, CTELNs were mixed with PKH67 and incubated for 10 min. Subsequently, PBS was added and the sample was centrifuged at 100,000× g for 1 h to remove the unbound-free dye. RAW 264.7 cells were seeded into 6-well plates and cultured until the cells adhered. The cells were then treated with 20 μg/ml PKH67-labeled

CTELNs and incubated for 3 h, 6 h, and 12 h, respectively. After incubation, the medium was discarded, and cells were fixed with 4% paraformaldehyde for 10 min. After three washes with PBS, the cells were stained with DAPI for 15 min. Following another three washes with PBS, the cells were observed under a fluorescence microscope (Nikon Ts2R).

2.11 Analysis of oxidative stress

RAW264.7 cells were inoculated into 6-well plates and assigned to different treatment groups. The cells in each group were collected by centrifugation at 5,000 rpm for 5 min, and the cell samples were incubated with 200 μL lysate on ice for 30 min. The antioxidant effect was determined using SOD kit, GSH-Px kit, and MDA kit according to the manufacturer's protocols. Each test was replicated 3 times.

2.12 Statistical analysis

Results are expressed as mean ± standard deviation (SD). Data were analysed by one-way analysis of variance (ANOVA) or Mann-Whitney U test using IBM SPSS Statistics software (version 26). Data graphing analysis was conducted by GraphPad Prism 10.3. The heatmap were mapped using ChiPlot (https://www.chiplot.online/). Relative quantitative analysis of intracellular fluorescence was performed using ImageJ software.

3. Results and discussion

3.1 Characteristics of CTELNs

CTELNs are primarily isolated through differential centrifugation, ultrafiltration, and PEG precipitation, with the operational workflow illustrated in Fig. 1A. To further characterize CTELNs, particle size and zeta potential were measured. As depicted in Fig. 1B, the particle size of the obtained CTELNs exhibited a PEG concentration-dependent decrease. Specifically, at PEG concentrations of 10%, 12%, 16%, 20%, and 30% (*w*/*v*), the mean particle sizes were 160.27 ± 4.78 nm, 148.63 ± 9.27 nm, 138.77 ± 3.55 nm, 125.50 ± 9.87 nm, and 118.63 ± 1.59 nm, respectively. These results were consistent with previous studies on plant-derived nanovesicles: the average size of tomato-derived vesicles was 160 ± 3 nm [5], the exosomes derived from follicular fluid showed a mean particle size of 134.8 nm [25], and electron microscope analysis showed the size of Citrus limon L. nanovesicles ranged from 50 to 70 nm [2]. Results revealed that CTELNs fell within the typical size range observed for plant-derived nanovesicles. Moreover, the CTELNs isolated using higher PEG concentrations (20% and 30%) exhibited significantly smaller particle sizes compared to those obtained with lower concentrations (10%, 12%, and 16%), highlighting PEG concentration as a critical parameter for particle size during isolation. This observation is consistent with a previous reports showing that elevated PEG concentrations preferentially precipitated smaller exosomes [26].

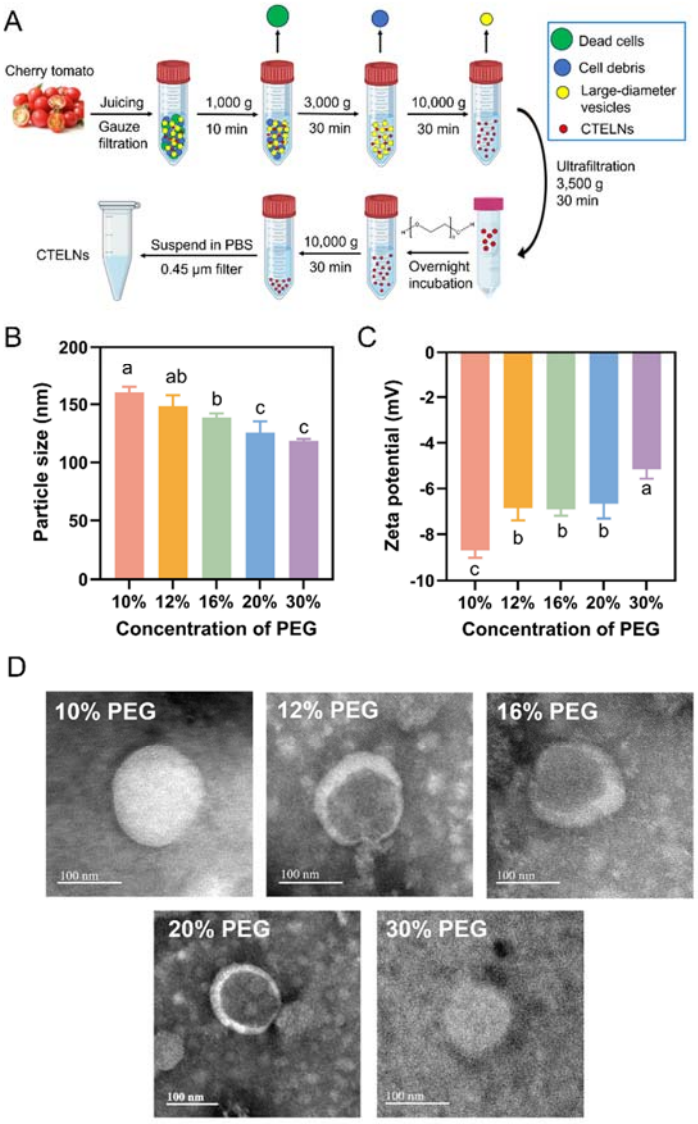

Fig. 1 Isolation flowchart (A), particle size (B), zeta potential (C) and representative TEM image (D) of the CTELNs isolated by the PEG precipitation method. The concentrations of PEG were 10%, 12%, 16%, 20%, and 30% (*w*/*v*), respectively. Different lowercase letters indicate significant differences, $P < 0.05$. The data represent the means ± standard deviations (SD) (n = 3). The scale bar = 100 nm.

Zeta potential serves as an indicator of the relative aggregation tendency and stability of nanoparticle suspensions. Similar values between -5 mV and -9 mV were observed (Fig. 1C). It was reported that blueberry-derived exosome-like nanoparticles had a negative zeta potential of -2.52 mV [21], the zeta potential of garlic-derived exosome-like nanoparticles was approximately -7.8 mV [27], and the average zeta potentials of two cabbage exosomes were -14.8 mV and -15.2 mV [28]. While these comparative data validate the measured zeta potential range, it is acknowledged that the PEG precipitation method may induce non-specific adsorption or conformational changes of surface biomolecules, potentially affecting the native charge distribution [29]. The zeta potential values suggest that CTELNs maintain reasonable stability despite potential PEG-induced surface charge perturbations.

The morphological characteristics of CTELNs were analyzed by TEM (Fig. 1D). All nanoparticles predominantly showed cup-shaped structure or spherical shapes with an average size of approximately 100 nm, consistent with the morphology of PELNs isolated by PEG [15]. Notably, TEM analysis revealed a

relatively smaller particle size distribution compared to NTA measurements. This size variation can be explained by their different measurement environments: NTA operates in aqueous solution where the expansion of surface-bound hydrophilic molecules is in aqueous environments, while TEM observation is performed under vacuum conditions [30].

3.2 Biochemical Composition of CTELNs

The quantitative analysis of the particle concentration in the harvested CTELNs fractions across a gradient of PEG concentrations showed that the particle yields were 1.56 ± 0.33×10^{10}/mL, 2.26 ± 0.14×10^{10}/mL, 2.35 ± 0.32×10^{10}/mL, 2.43 ± 0.20×10^{10}/mL, and 2.4 ± 0.20×10^{10}/mL, respectively (Fig. 2A). The results demonstrate a concentration-dependent enhancement in the particle yield, with the highest recovery observed within the 12 - 30% PEG range and the lowest yield was recorded at 5% PEG. This result is consistent with a previous study on EV isolated by PEG method from tissue culture media [15], where analysis of the pellets harvested per milliliter of conditioned medium revealed a PEG concentration dependence for all PEG variants. For PEG 8000, the highest pellet yield was achieved at a final concentration of 8 - 10 %.

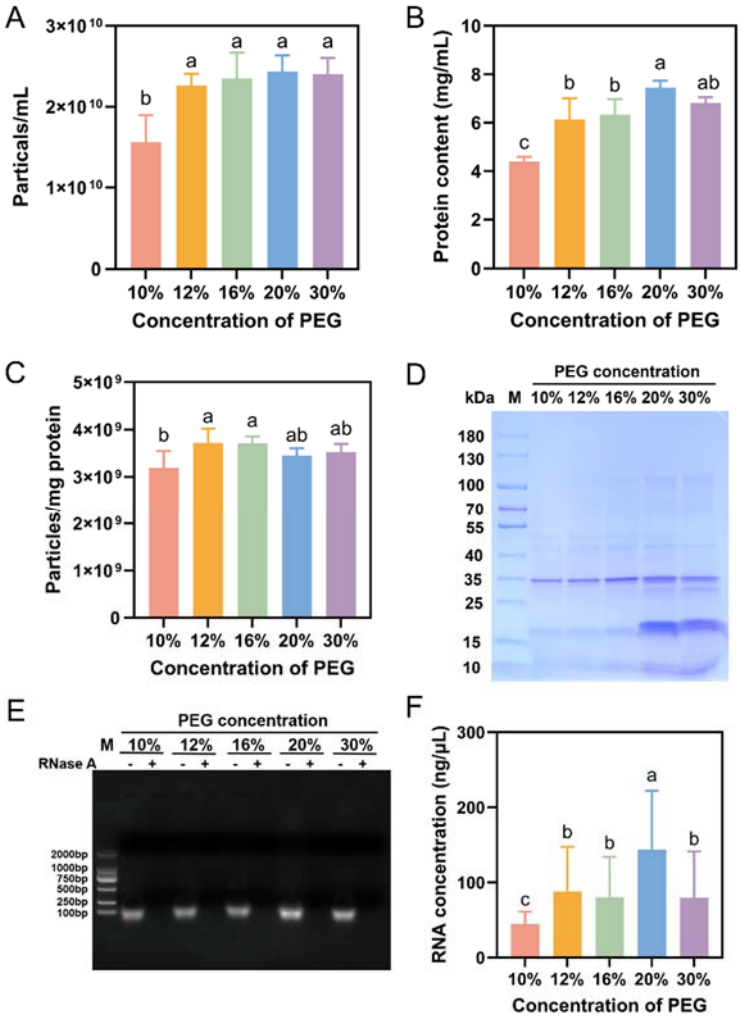

Fig. 2 Particle numbers (A), protein content (B), the purity (determined as particle numbers per μg protein content) (C), SDS-PAGE gel image (D), agarose gel electrophoresis (E) and RNA concentration (F) of the CTELNs isolated by the PEG precipitation method. The concentrations of PEG were 10%, 12%, 16%, 20%, and 30% (*w*/*v*), respectively. Different lowercase letters indicate significant differences, $P < 0.05$. The data represent the means ± standard deviations (SD) (n = 3).

The protein composition of exosomes differs based on their isolation source, however, they all contain specific proteins. To evaluate the protein cargo of CTELNs, we performed BCA assays on vesicle preparations obtained at the aforementioned PEG concentrations. As depicted in Fig. 2B, the total protein concentration of CTELNs ranged from 4.87 ± 0.55 mg/mL (10% PEG) to 7.45 ± 0.29 mg/mL (20% PEG), exhibiting a positive correlation with PEG dosage up to 20%. Beyond this threshold, protein levels plateaued (6.81 ± 0.24 mg/mL at 30% PEG). This result suggests that while moderate PEG concentrations enhance protein recovery through improved precipitation efficiency, high concentrations may lead to diminishing returns due to solution viscosity effects or protein solubility limits. BCA assays quantified *Pueraria lobata* Root-ELN protein concentrations at 5.28 ± 0.05 mg/mL [31]. The protein content at 20% PEG not only exceeds that in the Pueraria lobata Root-ELN, but also confirms the high protein content of CTELNs, supporting their potential as biologically active nanovesicles.

The ratio of particles to protein was calculated and utilized as an indicator of purity for the obtained CTELNs samples. As shown in Fig. 2C, the ratio increased from 3.19 ± 0.36×10^9 to a peak of 3.71 ± 1.46×10^9, indicating superior vesicle enrichment at intermediate PEG concentrations.

To gain further insights into the protein composition of CTELNs, SDS-PAGE analysis was performed. The SDS-PAGE result not only confirmed the presence of multiple proteins but also provided valuable information regarding their molecular weights [32]. Numerous clearly visible protein bands were evenly distributed throughout the gel, and their electrophoretic mobility revealed that the molecular weight of the proteins constituting the CTELNs ranged broadly from approximately 10 to 130 kDa (Fig. 2D). The gel exhibited a complex banding pattern, with three predominant regions of high intensity. A distinct band of high abundance was consistently observed at approximately 100 kDa. The most densely stained and concentrated cluster of major bands was localized in the 35 kDa region, suggesting the presence of several highly enriched protein species within this molecular weight range. Additionally, a clearly defined and prominent band was detected at 18 kDa. This even distribution of bands is indicative of a complex and diverse composition of proteins encapsulated within the CTELNs. The protein bands of tomato-derived exosomes are mainly distributed between 19 and 97 kDa, with the main bands located in 19, 35, 51, and 97 kDa [5]. The CTELNs displayed a similar but distinct profile. This molecular weight distribution pattern suggests conserved protein components among solanaceous plant-derived exosomes, while maintaining species-specific variations. This wide range of molecular weights underscores the complexity of the protein cargo within these nanoparticles, suggesting that they may contain multiple proteins with diverse functions and roles in cellular processes.

The biological functions of exosomes are mediated not only by their protein components but also through their RNA content. A study found that numerous miRNAs were present in 11 edible plant-derived ENPs, with these miRNAs being predicted to interact with the mammalian transcriptome [33]. Therefore, to investigate the RNA profile of the CTELNs isolated using PEG precipitation, we performed total RNA analysis. In this study, the agarose gel analysis confirmed the presence of RNA in CTELNs, predominantly consisting of small RNA

with a length of 100 bp (Fig. 2E). Pretreatment of the CTELNs with RNase A led to the elimination of the bands, thus validating the RNA composition of the observed bands. The highest RNA concentration in the 20% PEG-isolated CTELNs (143.63 ± 78.44 ng/μL, Fig. 2F), was 3.3-, 1.6-, 1.8-, and 1.8-fold higher than those obtained with 10%, 12%, 16%, and 30% PEG, respectively. The results are consistent with a previous research [27], indicating that RNA is a critical functional component of CTELNs.

The comparative analysis revealed that the CTELNs isolated using 20% PEG exhibited superior physicochemical properties, including stability, protein content and RNA content. Based on these findings, 20% PEG was identified as the optimal concentration for CTELNs isolation and consequently employed in all subsequent experiments.

3.3 The miRNA profiling and functional annotation of CTELNs

Given that PELNs contain a variety of miRNAs which may serve as bioactive mediators of cross-kingdom communication [34], the CTELNs isolated by 20% PEG were subjected to small RNA sequencing, yielding 7.2 million clean tags from three CTELNs samples (Table 1). As shown in Fig. 3A, the length range of cherry tomato and CTELNs was 16-30 nt, and the small RNAs in cherry tomato tissue were dominantly distributed between 21 and 28 nt, while the most abundant small RNAs were distributed in the range of 23-24 nt in CTELNs, consistent with the length distribution of plant miRNA [35]. A total of 222 miRNAs were identified in CTELNs and cherry tomato samples, of which 125 miRNAs were commonly found in both samples, 4 miRNAs were only present in CTELNs, and 93 were only found in cherry tomatoes (Fig. 3B). There were 88 differentially expressed miRNAs between CTELNs and tissue, including 57 upregulated and 31 downregulated miRNAs (Fig. 3C-E).

Table 1 Summary of small RNA sequencing data.

Sample	Total Reads	Clean Reads	Low Quality Reads	GC content (%)	Q20 (%)
Cherry tomato 1	47,341,534	20,293,391	206,398	50.24	99.1
Cherry tomato 2	27,848,101	21,954,431	112,567	48.15	99.1
Cherry tomato 3	44,986,057	18,764,304	239,445	48.68	99.0
CTELNs 1	26,274,450	24,336,568	128,174	46.08	98.9
CTELNs 2	27,042,765	25,237,475	158,110	45.80	98.9
CTELNs 3	25,665,841	23,234,761	79,474	46.61	99.2

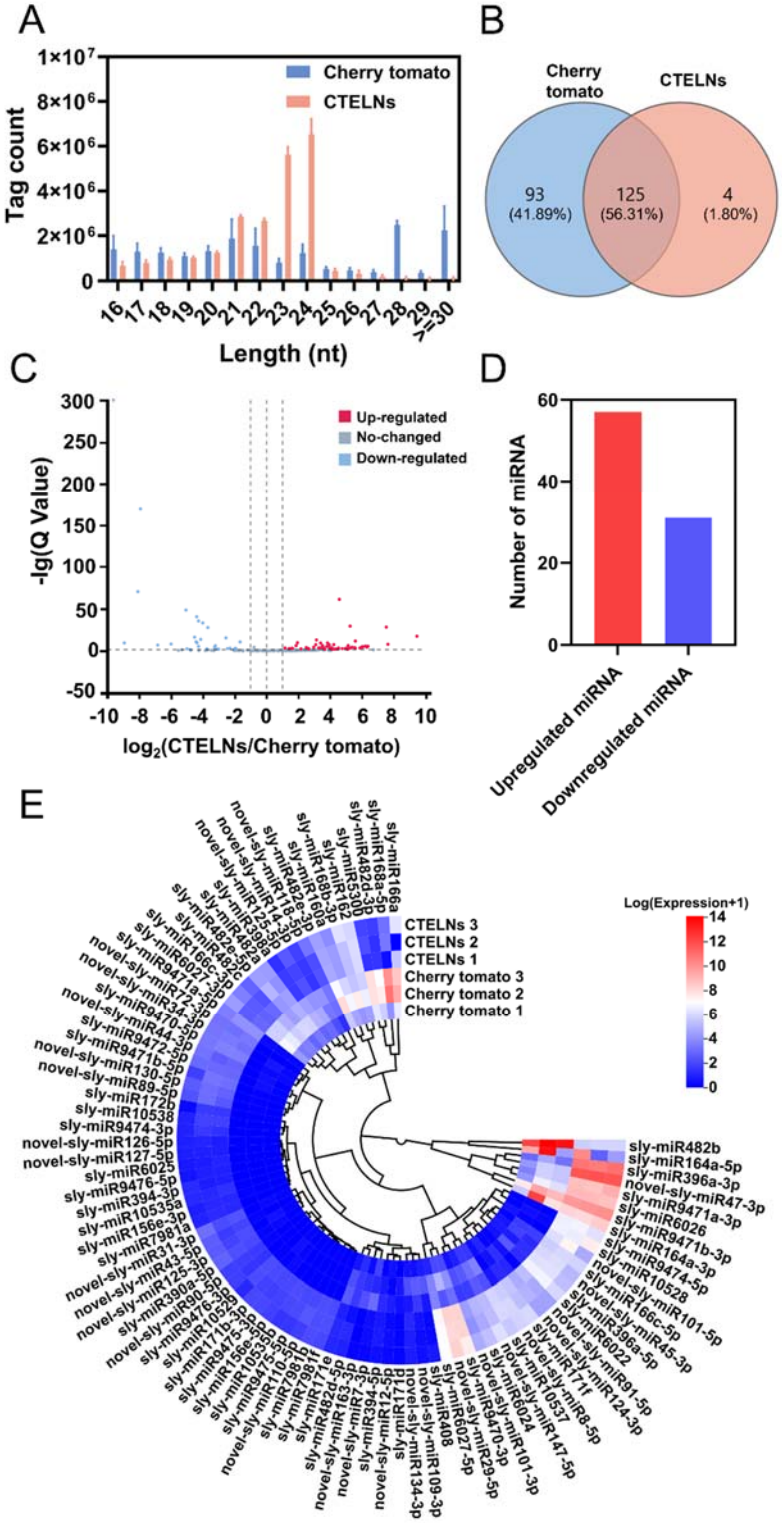

Fig. 3 The length distribution of small RNA (A), venn diagram of known miRNAs and novel miRNAs (B), volcano plot (C), number (D) and heatmap (E) of differential miRNAs in CTELNs and cherry tomato. Blue represents downregulation, and red represents upregulation.

The KEGG results showed that the most enriched pathways were related to carbohydrate metabolism, global and overview maps, and transport and catabolism (Fig. 4A). GO annotation revealed that the predicted target genes of CTELNs-derived miRNAs were significantly enriched in biological processes related to oxidative stress. In the biological process, the predicted targets were mainly associated with the cellular process, metabolic process, biological regulation, regulation of biological processes, and response to

stimulus. The most abundant GO terms in molecular function were binding and catalytic activity (Fig. 4B), which were critical for the antioxidant responses, such as the binding of transcription factors to antioxidant response elements [36] and the catalytic elimination of reactive oxygen species (ROS) [37].

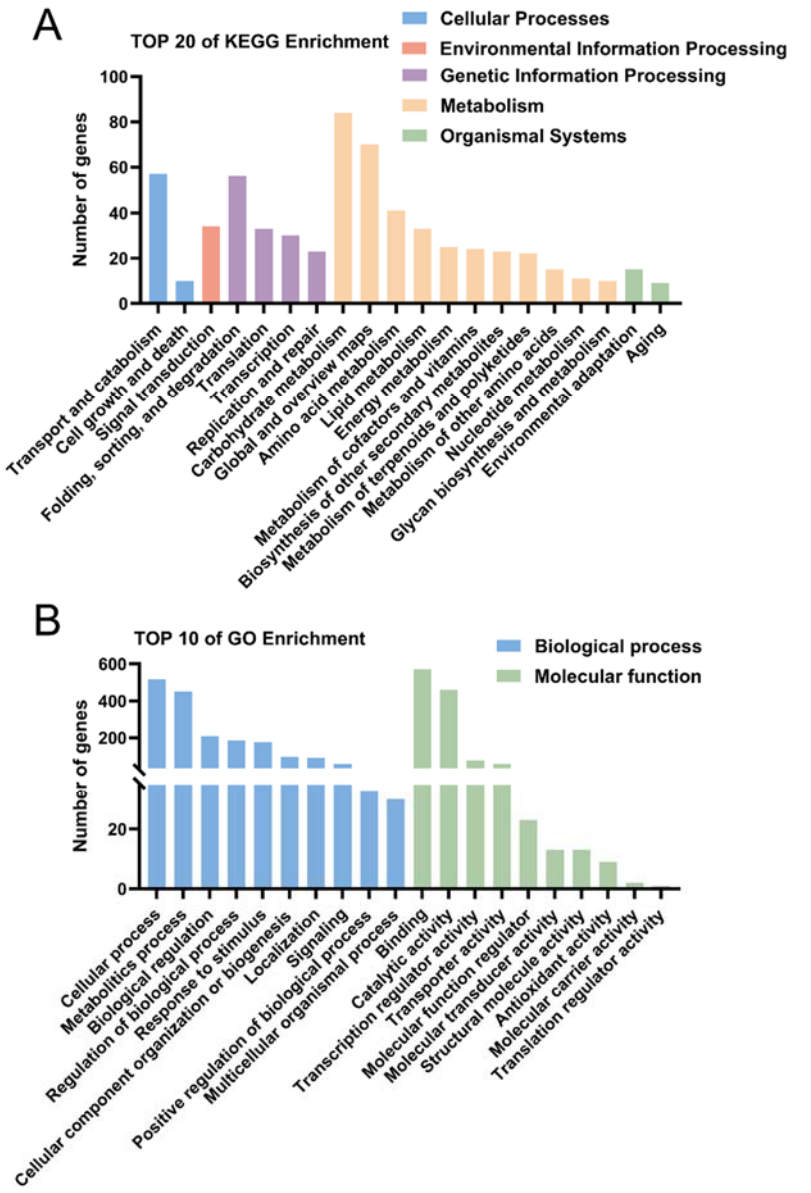

Fig. 4 KEGG enrichment analysis (A) and GO enrichment analysis (B) of target miRNA genes in CTELNs.

Since the enriched pathways were related to antioxidant response, further analyses were focused on several miRNAs functionally associated with oxidative stress (Fig. 5). Specifically, miR156e-3p, miR156e-5p, miR390a-5p, and miR9474-5p were identified as significantly abundant in CTELNs compared to cherry tomato tissue (Fig. 5A-D), which were primarily involved in binding and catalytic activity (Table 2). Interestingly, these enriched miRNAs have been previously reported to be implicated in the regulation of oxidative stress and antioxidant mechanisms. For instance, miR156 was found to promote anthocyanin accumulation in transgenic Arabidopsis overexpressing miR156e from herbaceous peony [38]. Anthocyanins enhanced antioxidant capacity not only by directly scavenging free radicals but also by upregulating the activity of key antioxidant enzymes, such as SOD and catalase [39]. Similarly, miR390-overexpression has been shown to enhance resistance to fungal stress by elevating the activity of antioxidant enzymes in plants

[40], while miR9474-5p was involved in fruit responses to oxidative and environmental stimuli [41]. The presence of these miRNAs further underscores the potential of CTELNs in cellular biology and therapeutic applications.

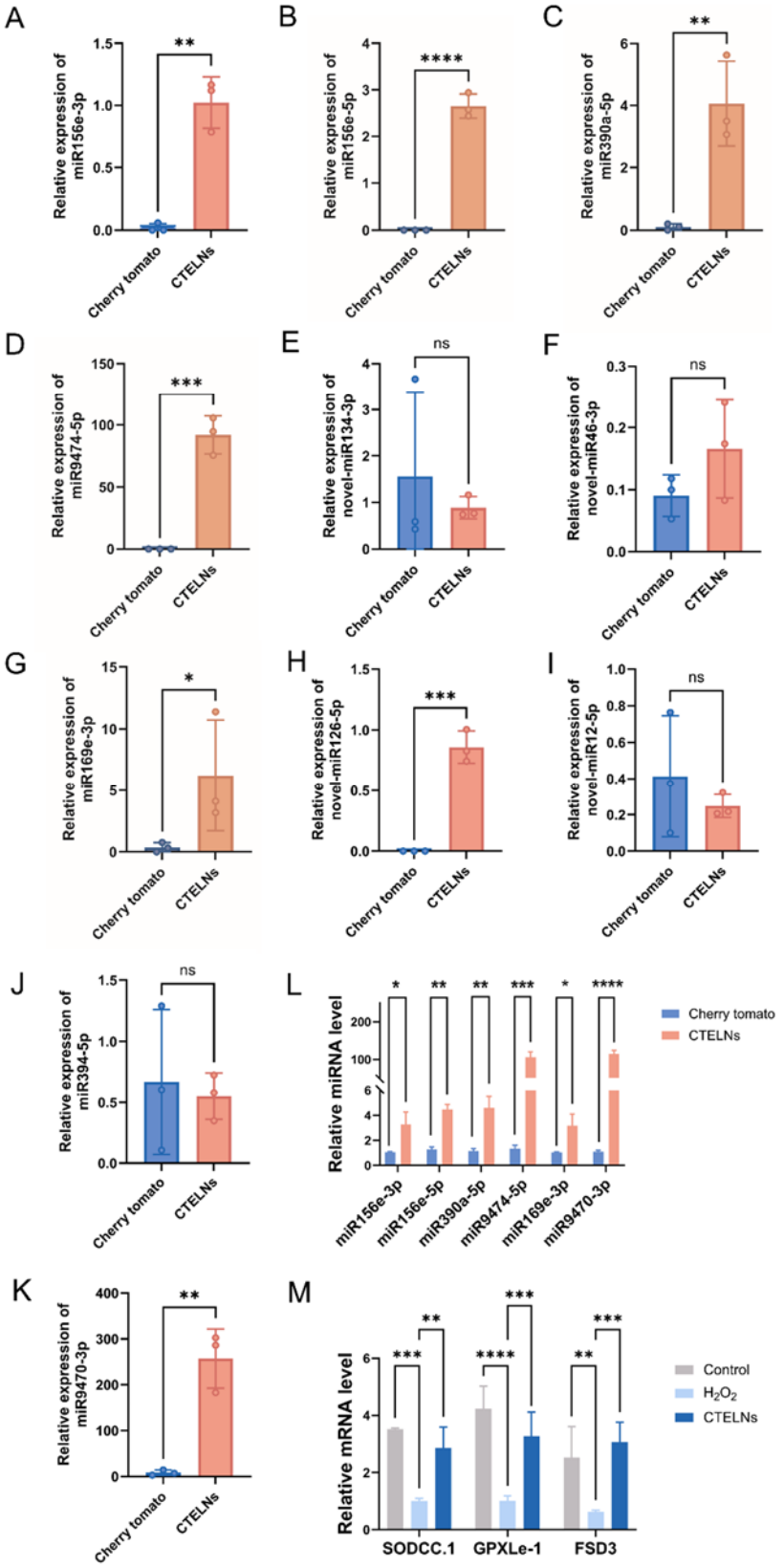

Fig. 5 (A-K) Relative expression of miRNAs related to oxidative stress. (L) Expression profiles of six miRNAs in CTELNs and cherry tomato. (M) The expression levels of oxidative genes, including SODCC.1, GPXLe-1, and FSD3, in H_2O_2-induced RAW264.7 cells. The data represent the means ± standard deviations (SD) (n = 3). * $P < 0.05$, ** $P < 0.01$, *** $P < 0.001$, ns represents no significant difference.

Table 2 Selected miRNAs related to oxidative stress and GO annotation.

miRNA	Predicted target genes	GO annotation
miR156e-3p	Chorismate mutase	Catalytic activity
miR156e-5p	TH2; SBP3; SPL; CBP60	Biological regulation; Binding
miR390a-5p	PXC3; LRR	Binding; Catalytic activity
miR9474-5p	MANBA; PPAN; NADH	Biological regulation; Binding; Catalytic activity

The prediction of miRNA target genes is essential for evaluating their biological functions and mechanisms. Therefore, beyond these individually characterized miRNAs, the analysis uncovered an antioxidant activity term in GO annotation consisting of nine enriched miRNAs (Fig. 5E-K). To validate the reliability of the RNA-seq data, six miRNAs were selected and analyzed for qRT-PCR confirmation. The expression trends determined by qRT-PCR were in strong agreement with the RNA-seq results (Fig. 5L), confirming the reliability of sequencing data for subsequent analysis. This set of miRNAs was bioinformatically predicted to target key endogenous antioxidant enzymes, including SOD and GSH-Px (Table 3), which are the core executors of cellular defense against oxidative damage [42]. In order to identify the specific target mRNA responsible for the observed effects, expression of the genes related to oxidative stress was used by qRT-PCR. As shown in Fig. 5M, compared to the control group, the relative mRNA expression levels of SODCC.1, GPXLe-1, and FSD3 in the H_2O_2-induced group were significantly decreased, which was consistent with a previous report [43]. Interestingly, the changes in mRNA expression levels of SODCC.1, GPXLe-1, and FSD3 by H_2O_2 were reversed by treatment with CTELNs. Collectively, the findings established that CTELNs were enriched with specific miRNAs functionally linked to oxidative stress regulation and were predicted to target antioxidant genes, thereby regulating antioxidant response mechanisms.

Table 3 Selected miRNAs and predicted target genes related to oxidative stress based on GO enrichment.

miRNA	Predicted target genes	KEGG pathway
novel-miR134-3p novel-miR46-3p	SODCC.1	Transport and catabolism, Aging
miR169e-3p novel-miR126-5p	GPXLe-1	Metabolism of other amino acids, Lipid metabolism
novel-miR12-5p	APX2	Carbohydrate metabolism, Metabolism of other amino acids
miR482e-3p	FSD3	Transport and catabolism, Aging
miR394-5p	PER7	Biosynthesis of other secondary metabolites
novel-miR163-3p	PER42	
miR9470-3p	PER64	

3.4 Cellular responses to CTELNs

CCK-8 assay and LDH release assay were employed to evaluate the cytotoxicity of CTELNs in RAW264.7 cells (Fig. 6). The cells were treated with increasing concentrations of CTELNs (0, 5, 10, 20, and 40 μg/mL, normalized by protein content) and assessed at 24 h and 48 h to examine dose- and time-dependent effects. According to the cell viability and cellular toxicity (Fig. 6), even at the highest concentration, cellular toxicity was not observed and CTELNs did not induce any significant reduction in cell viability. Importantly, this non-cytotoxic profile was maintained regardless of PEG concentration or incubation duration, with all treatment groups maintaining > 95% viability relative to controls. The findings indicated that CTELNs exposed no toxicity to RAW264.7 cells, consistent with numerous studies confirming the nontoxic nature of PELNs. For example, pomegranate ELNs at 2.5 to 20 μg/mL had no significant toxic effects on Caco-2 cells [44], and blueberry ELNs at 0-40 μg/mL did not alter the cell viability of EA.hy926 cells [45]. These results demonstrate that CTELNs exhibited excellent biocompatibility with RAW264.7 cells, showing no significant cytotoxic effects across a wide range of concentrations and exposure times, thereby supporting their potential for therapeutic applications.

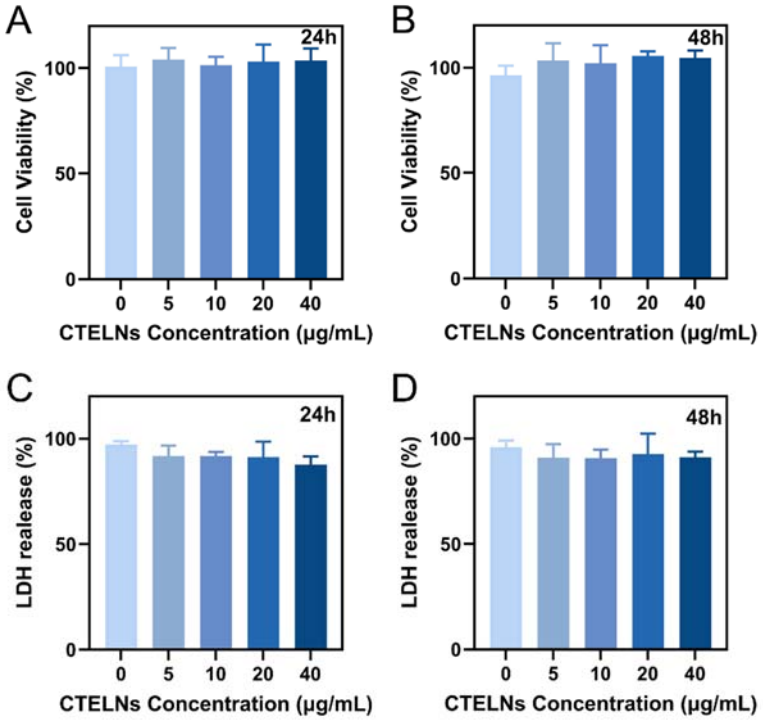

Fig. 6 The cell viability (A-B) and cellular toxicity (C-D) of RAW264.7 cells after CTELNs treatment. CTELNs was isolated by 20% PEG (*w*/*v*) precipitation method. No significant difference was observed between the groups. The data represent the means ± standard deviations (SD) (n = 3).

To monitor the dynamic uptake of CTELNs, RAW264.7 cells were incubated with PKH67-labeled CTELNs and observed at 3 h, 6 h, and 12 h. As shown in Fig. 7, green fluorescence was detected inside the cells at 3 h. After 6 h incubation, scattered green puncta appeared in the perinuclear region, suggesting initial internalization of CTELNs. Following 12 h of exposure, abundant green fluorescent signals accumulated predominantly around the nucleus, indicating substantial intracellular entry and perinuclear accumulation of CTELNs in RAW264.7 cells.

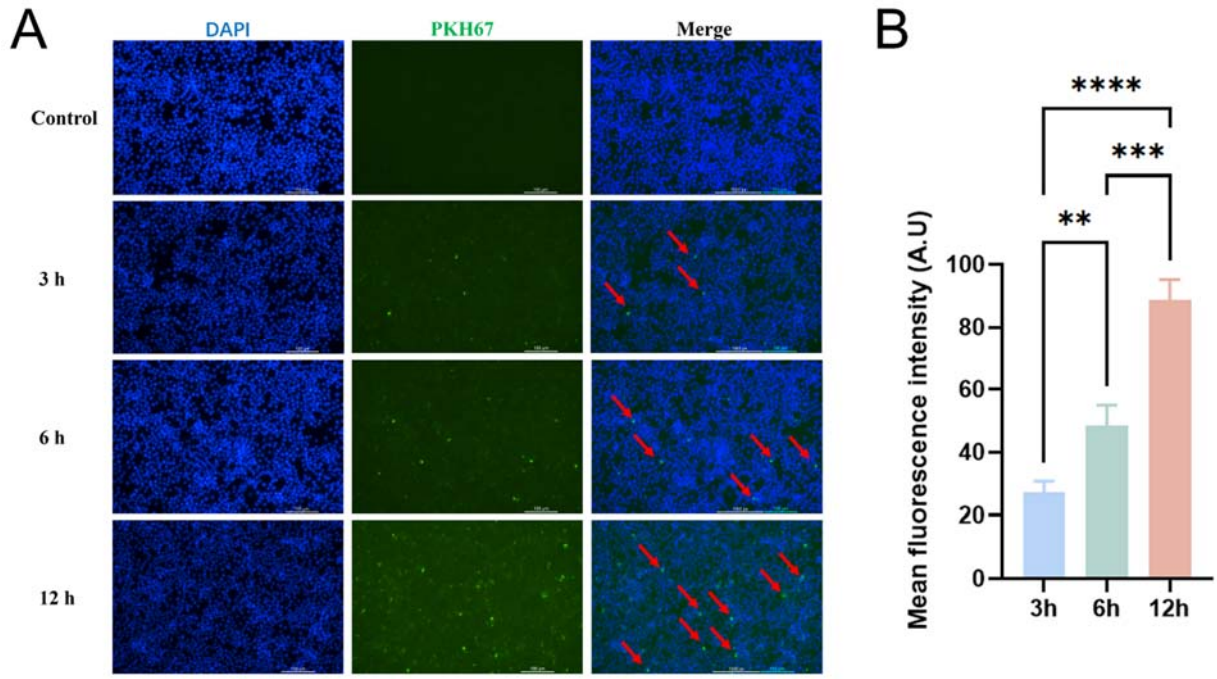

Fig. 7 Fluorescence microscopy images (A) and mean fluorescence intensity (B) of Raw264.7 cells incubated with the 20 μg/mL CTELNs for 3 h, 6 h and 12 h. Raw 264.7 cell nuclear were labeled with DAPI (blue), CTELNs were labeled with PKH67 (green). Representative images were collected using 20× resolution (bar=100μm). The data represent the means ± standard deviations (SD) (n = 3). * $P < 0.05$, ** $P < 0.01$, *** $P < 0.001$, ns represents no significant difference.

Exosomes are enriched with antioxidant bioactive molecules that effectively scavenge ROS and other free radicals, thereby mitigating oxidative stress and inhibiting apoptosis [10]. Notably, SOD catalyzes the dismutation of superoxide radicals into hydrogen peroxide (H_2O_2) and molecular oxygen, thereby maintaining redox homeostasis and thus ensuring cell viability [46]. GSH-Px serves as a critical intracellular antioxidant enzyme that mitigates oxidative stress by catalyzing the reduction reaction of reduced glutathione to H_2O_2, thereby protecting cellular macromolecules from peroxidative damage [47]. The level of MDA is widely used as a surrogate biomarker to assess the extent of oxidative stress-induced cellular lipid damage [48]. Therefore, based on the findings that miRNAs may target antioxidant enzymes, the effects of the CTELNs isolated by 20% PEG on SOD, GSH-Px, and MDA were determined for validation.

A previous study has found that 300 μM H_2O_2 effectively induced oxidative damage [25], we employed this concentration to stimulate RAW264.7 cells and evaluate the therapeutic effect of CTELNs on oxidative stress (Fig. 8A), with their antioxidant activity being determined by measuring the activities of SOD and GSH-Px and MDA level (Fig. 8B-D). The oxidative stress model established by 300 μM H_2O_2 treatment reduced SOD activity in RAW264.7 cells to 28.96 ± 3.91 U/mg protein ($P<0.05$) (Fig. 8B). Treatment with 10 μg/mL CTELNs significantly restored SOD activity to 46.90 ± 4.98 U/mg protein ($P<0.01$), which was not significantly different from the control group. Notably, 40 μg/mL CTELNs (approximately 1.3×10^8 particles/mL based on our particle-protein correlation) further enhanced this effect, elevating SOD activity to 50.91 ± 6.43 U/mg protein. These results not only demonstrated a dose-dependent antioxidant capacity of CTELNs, but also revealed their superior efficacy compared to flos Puerariae-derived exosome-like nanoparticles, which were reported to restore SOD activity from 20 U/mg protein to approximately 40 U/mg

protein [49]. Treatment with aloe vera gel-derived exosome-like nanoparticles significantly increased SOD activity by approximately 25% *in vivo* [50], whereas CTELNs treatment resulted in a more pronounced increase of approximately 75%. These findings suggest that CTELNs may possess a stronger potential in enhancing antioxidant defense, and future studies will further validate the efficacy and underlying mechanisms of CTELNs action *in vivo*.

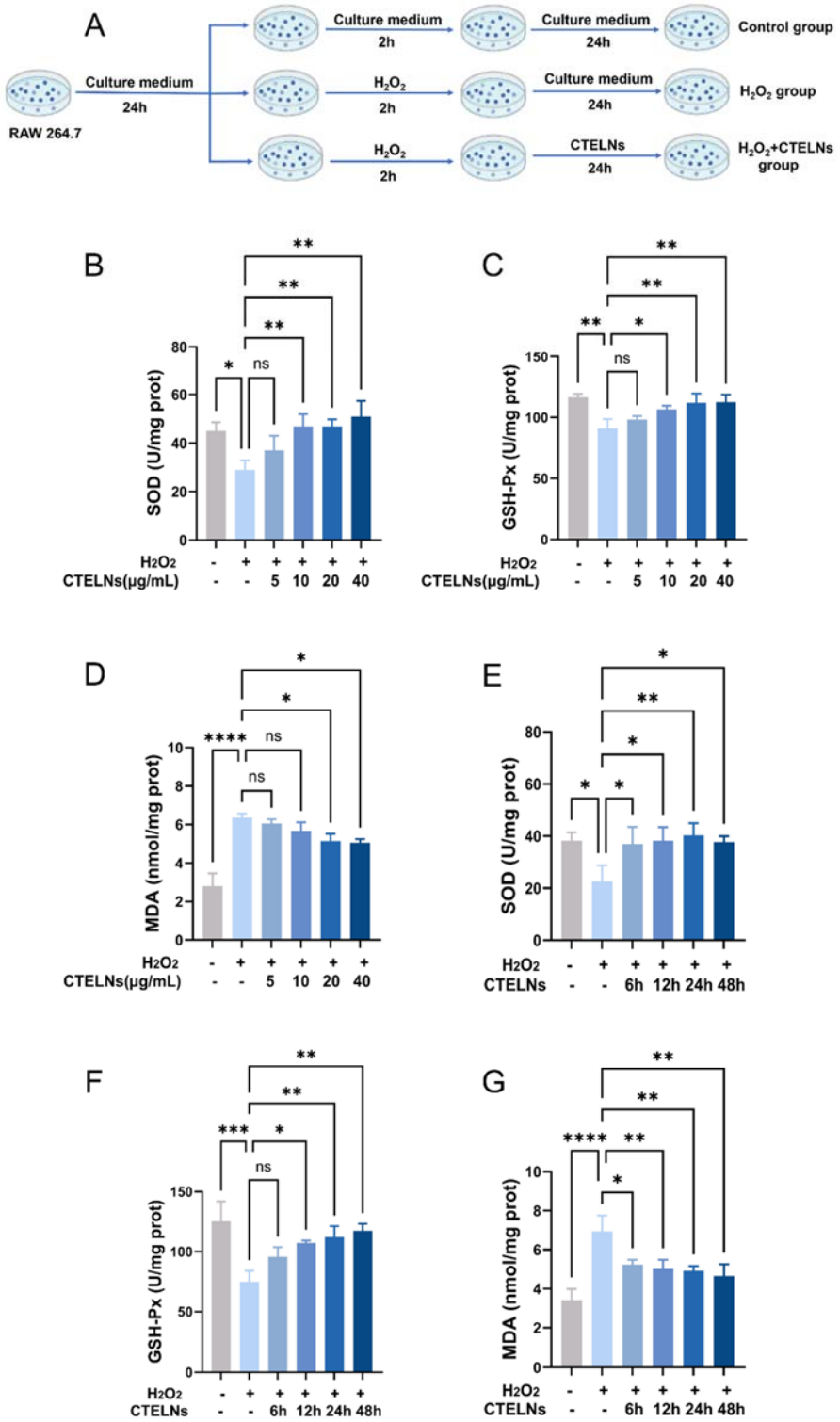

Fig. 8 Concentration- and time-dependent antioxidant activity of CTELNs *in vitro*. (A) Roadmap of experimental design. (B-D) Effects of CTELNs on the levels of SOD, GSH-Px, and MDA in RAW264.7 cells stimulated with 300 μM H_2O_2 for 2 h. (E-G) Effects of 20 μg/mL CTELNs on the activities of SOD and GSH-Px, and MDA level in RAW264.7 cells with 300 μM H_2O_2 stimulation. The data represent the means ± standard deviations (SD) (n = 3). * $P < 0.05$, ** $P < 0.01$, *** $P < 0.001$, ns represents no significant difference.

As shown in Fig. 8C, H_2O_2 treatment reduced GSH-Px activity in RAW264.7 cells from 116.44 ± 2.72 U/mg protein to 90.97 ± 7.66 U/mg protein compared to the control group. CTELNs treatment exhibited a concentration-dependent restorative effect on GSH-Px activity, with 10 μg/mL and 40 μg/mL treatments increasing the activity by 1.17-fold and 1.24-fold, respectively, though these values did not differ significantly from the control levels. Similarly, it was reported that 10 μg mesenchymal stem cells (MSCs) extracellular vesicles elevated GSH-Px activity by 1.5-fold in hippocampal neuron [23].

As shown in Fig. 8D, H_2O_2 treatment induced a 3-fold increase in intracellular lipid peroxidation compared to the control group. CTELNs treatment effectively reduced MDA levels in a concentration-dependent manner. Notably, 20 μg/mL and 40 μg/mL CTELNs treatments for 24 h decreased MDA levels by 1.24-fold and 1.3-fold, respectively ($P<0.05$), which compared favorably with the 1.1-fold reduction achieved by 20 μg/mL Opuntia ficus-indica fruit-EVs under similar experimental conditions [51]. It was reported that 50 μg/mL beta vulgaris-derived exosomes reduced MDA content by 16.67% [52], while 40 μg/mL CTELNs treatment demonstrated a more pronounced inhibitory effect, lowering MDA levels by 20%, indicating that CTELNs exhibit superior efficacy in mitigating H_2O_2-induced lipid peroxidation in this cellular model.

In addition, based on concentration-dependent antioxidant experiments described above, we further performed the temporal effects of 20 μg/mL CTELNs isolated by 20% PEG on H_2O_2-induced oxidative stress (Fig. 8E-G). Initial improvements were observed within 6 h, with enhancement in SOD activity (Fig. 8E) and reduction in MDA levels ($P<0.05$) (Fig. 8G), while GSH-Px activity (Fig. 8F) showed a delayed response, becoming statistically significant only after 12 h (107.15 ± 2.00 U/mg protein, 1.43-fold increase versus the H_2O_2 group). The antioxidant efficacy reached maximal potency at 48 h, demonstrating coordinated upregulation of SOD (37.69 ± 2.29 U/mg protein, 1.68-fold increase) and GSH-Px (117.30 ± 5.93 U/mg protein, 1.57-fold increase) activities coupled with substantial suppression of lipid peroxidation (4.66 ± 0.60 nmol/mg protein, 1.49-fold reduction).

Overall, the results from both concentration and time-course experiments collectively demonstrate that the biological activity of CTELNs, as a novel type of natural nanoparticle, provides crucial theoretical foundation and feasibility for their future exploration and development in functional foods or oral delivery systems.

4. Conclusions

In summary, a comparative analysis of CTELNs isolated using different PEG concentrations revealed that those obtained with 20% PEG exhibited superior characteristics in terms of particle size distribution, morphology, and purity. Moreover, CTELNs were also rich in complex proteins and RNA. The small RNA sequencing data established that CTELNs were enriched with a critical set of miRNAs functionally linked to the oxidative stress response. Target gene prediction indicates that the miRNA may play a crucial role in regulating cellular oxidative stress responses by modulating gene expression. Furthermore, cellular experiments demonstrated the non-toxic nature and antioxidant capacity of CTELNs. Cytotoxicity

assessments revealed that CTELNs treatments maintained > 95% cell viability over 48h. Antioxidant activity was validated using H_2O_2 induced oxidative stress models, wherein CTELNs treatment enhanced SOD and GSH-Px activity while decreasing MDA content.

However, a main limitation of the current work must be acknowledged. The mechanistic insights were derived primarily from *in vitro* models, and so the physiological relevance and bioavailability of CTELNs upon oral administration remained to be validated by *in vivo* systems. Subsequent studies should prioritize evaluating the pharmacokinetics, biodistribution, and efficacy of CTELNs in relevant animal models. Collectively, CTELNs offer several advantages, including low toxicity, cost-effectiveness, and abundant biological activity, providing a theoretical basis for the application of plant derived exosome-like nanoparticles in biomedical fields. Notwithstanding these future challenges, the findings illuminate that CTELNs represent a promising candidate for development as a biocompatible vehicle for the oral delivery of therapeutic agents.

Declaration of competing interest

The authors declare that they have no known competing financial interests or personal relationships that could have appeared to influence the work reported in this paper.

Data availability

Data will be made available on request.

Acknowledgment

This work was supported by Tianjin Science and Technology Planning Project [grant number 25JCZDJC00460, 23ZYCGSN00930, and 24YFZCSN00320]. The authors are grateful to Haitao Li and Ruiqi Sun for their help in this research.

References

[1] L. Doyle, M. Wang, Overview of Extracellular Vesicles, Their Origin, Composition, Purpose, and Methods for Exosome Isolation and Analysis, Cells. 8(7) (2019) 727. https://doi.org/10.3390/cells8070727.

[2] S. Raimondo, F. Naselli, S. Fontana, et al., Citrus limon -derived nanovesicles inhibit cancer cell proliferation and suppress CML xenograft growth by inducing TRAIL-mediated cell death, Oncotarget; . 6(23) (2015) 19514-27. https://doi.org/10.18632/oncotarget.4004.

[3] M. Zhang, E. Viennois, M. Prasad, et al., Edible ginger-derived nanoparticles: A novel therapeutic approach for the prevention and treatment of inflammatory bowel disease and colitis-associated cancer, Biomaterials. 101(2016) 321-40. https://doi.org/10.1016/j.biomaterials.2016.06.018.

[4] S. Ju, J. Mu, T. Dokland, et al., Grape Exosome-like Nanoparticles Induce Intestinal Stem Cells and Protect Mice From DSS-Induced Colitis, Molecular Therapy. 21(7) (2013) 1345-57. https://doi.org/10.1038/mt.2013.64.

[5] R. Mammadova, S. Maggio, I. Fiume, et al., Protein Biocargo and Anti-Inflammatory Effect of Tomato Fruit-Derived Nanovesicles Separated by Density Gradient Ultracentrifugation and Loaded with Curcumin, Pharmaceutics. 15(2) (2023) 333. https://doi.org/10.3390/pharmaceutics15020333.

[6] M. Distefano, E. Arena, R.P. Mauro, et al., Effects of Genotype, Storage Temperature and Time on Quality and Compositional Traits of Cherry Tomato, Foods. 9(12) (2020) 1729. https://doi.org/10.3390/foods9121729.

[7] Novelina, N. Nazir, M.R. Adrian, The Improvement Lycopene Availability and Antioxidant Activities of Tomato (Lycopersicum Esculentum, Mill) Jelly Drink, Agriculture and Agricultural Science Procedia. 9(2016) 328-34. https://doi.org/10.1016/j.aaspro.2016.02.144.

[8] J.-G. Mun, D.-H. Song, J.-Y. Kee, et al., Recent Advances in the Isolation Strategies of Plant-Derived Exosomes and Their Therapeutic Applications, Current Issues in Molecular Biology. 47(3) (2025) 144. https://doi.org/10.3390/cimb47030144.

[9] T.X. Lu, M.E. Rothenberg, MicroRNA, Journal of Allergy and Clinical Immunology. 141(4) (2018) 1202-7. https://doi.org/10.1016/j.jaci.2017.08.034.

[10] W. Zhang, R. Liu, Y. Chen, et al., Crosstalk between Oxidative Stress and Exosomes, Oxidative Medicine and Cellular Longevity. 2022(1) (2022) 3553617. https://doi.org/10.1155/2022/3553617.

[11] Y. Yan, W. Jiang, Y. Tan, et al., hucMSC Exosome-Derived GPX1 Is Required for the Recovery of Hepatic Oxidant Injury, Molecular Therapy. 25(2) (2017) 465-79. https://doi.org/10.1016/j.ymthe.2016.11.019.

[12] A. Ahmad, S. Fang, H. Tian, et al., Clinical application of a microfluidic chip for immunocapture and quantification of circulating exosomes to assist breast cancer diagnosis and molecular classification, Plos One. 12(4) (2017) e0175050. https://doi.org/10.1371/journal.pone.0175050.

[13] F. Perut, L. Roncuzzi, S. Avnet, et al., Strawberry-Derived Exosome-Like Nanoparticles Prevent Oxidative Stress in Human Mesenchymal Stromal Cells, Biomolecules. 11(1) (2021) 87. https://doi.org/10.3390/biom11010087.

[14] M.-C. López de las Hazas, J. Tomé-Carneiro, L. del Pozo-Acebo, et al., Therapeutic potential of plant-derived extracellular vesicles as nanocarriers for exogenous miRNAs, Pharmacological Research. 198(2023). https://doi.org/10.1016/j.phrs.2023.106999.

[15] A.K. Ludwig, K. De Miroschedji, T.R. Doeppner, et al., Precipitation with polyethylene glycol followed by washing and pelleting by ultracentrifugation enriches extracellular vesicles from tissue culture supernatants in small and large scales, Journal of Extracellular Vesicles. 7(1) (2018) 1528109. https://doi.org/10.1080/20013078.2018.1528109.

[16] Y. Zhang, J. Bi, J. Huang, et al., Exosome: A Review of Its Classification, Isolation Techniques, Storage, Diagnostic and Targeted Therapy Applications, International Journal of Nanomedicine. Volume 15(2020) 6917-34. https://doi.org/10.2147/ijn.S264498.

[17] M. Tangwattanachuleeporn, P. Muanwien, Y. Teethaisong, et al., Optimizing Concentration of Polyethelene Glycol for Exosome Isolation from Plasma for Downstream Application, Medicina. 58(11) (2022) 1600. https://doi.org/10.3390/medicina58111600.

[18] K.K. Sarwareddy, A.D. Singh, S. Patnam, et al., Harnessing tomato-derived small extracellular vesicles as drug delivery system for cancer therapy, Future Science OA. 11(1) (2025) 2461956. https://doi.org/10.1080/20565623.2025.2461956.

[19] E. Zeringer, T. Barta, M. Li, et al., Strategies for Isolation of Exosomes, Cold Spring Harbor Protocols. 2015(4) (2015) 319-23. https://doi.org/10.1101/pdb.top074476.

[20] R. Di Raimo, D. Mizzoni, M. Spada, et al., Oral Treatment with Plant-Derived Exosomes Restores Redox Balance in H2O2-Treated Mice, Antioxidants. 12(6) (2023) 1169. https://doi.org/10.3390/antiox12061169.

[21] W.-j. Zhao, Y.-p. Bian, Q.-h. Wang, et al., Blueberry-derived exosomes-like nanoparticles ameliorate nonalcoholic fatty liver disease by attenuating mitochondrial oxidative stress, Acta Pharmacologica Sinica. 43(3) (2021) 645-58. https://doi.org/10.1038/s41401-021-00681-w.

[22] K.J. Livak, T.D. Schmittgen, Analysis of Relative Gene Expression Data Using Real-Time Quantitative PCR and the 2−ΔΔCT Method, Methods. 25(4) (2001) 402-8. https://doi.org/https://doi.org/10.1006/meth.2001.1262.

[23] Q. Luo, P. Xian, T. Wang, et al., Antioxidant activity of mesenchymal stem cell-derived extracellular vesicles restores hippocampal neurons following seizure damage, Theranostics. 11(12) (2021) 5986-6005. https://doi.org/10.7150/thno.58632.

[24] V. Vanessa, H. Rachmawati, A. Barlian, Anti-inflammatory potential of goldenberry-derived exosome-like nanoparticles in macrophage polarization, Future Sci OA. 10(1) (2024) Fso943. https://doi.org/10.2144/fsoa-2023-0172.

[25] B. Pan, X. Li, Q. Yang, et al., Exosomes derived from follicular fluid promote proliferation and suppress apoptosis of yak (Bos grunniens) granulosa cells by enhancing antioxidant capacity in vitro, Animal Reproduction Science. 274(2025) 107790. https://doi.org/10.1016/j.anireprosci.2025.107790.

[26] M.A. Rider, S.N. Hurwitz, D.G. Meckes, ExtraPEG: A Polyethylene Glycol-Based Method for Enrichment of Extracellular Vesicles, Scientific Reports. 6(1) (2016) 23978. https://doi.org/10.1038/srep23978.

[27] J. Liu, W. Li, Y. Bian, et al., Garlic-derived exosomes regulate PFKFB3 expression to relieve liver dysfunction in high-fat diet-fed mice via macrophage-hepatocyte crosstalk, Phytomedicine. 112(2023) 154679. https://doi.org/10.1016/j.phymed.2023.154679.

[28] J.Y. You, S.J. Kang, W.J. Rhee, Isolation of cabbage exosome-like nanovesicles and investigation of their biological activities in human cells, Bioactive Materials. 6(12) (2021) 4321-32. https://doi.org/10.1016/j.bioactmat.2021.04.023.

[29] C. Bai, J. liu, X. Zhang, et al., Research status and challenges of plant-derived exosome-like nanoparticles, Biomedicine & Pharmacotherapy. 174(2024) 116543. https://doi.org/10.1016/j.biopha.2024.116543.

[30] D. Lin, W. Lin, G. Gao, et al., Purification and characterization of the major protein isolated from Semen Armeniacae Amarum and the properties of its thermally induced nanoparticles, International Journal of Biological Macromolecules. 159(2020) 850-8. https://doi.org/10.1016/j.ijbiomac.2020.05.070.

[31] W. Zhang, Q. Song, X. Bi, et al., Preparation of Pueraria lobata Root-Derived Exosome-Like Nanovesicles and Evaluation of Their Effects on Mitigating Alcoholic Intoxication and Promoting Alcohol Metabolism in Mice, International Journal of Nanomedicine. Volume 19(2024) 4907-21. https://doi.org/10.2147/ijn.S462602.

[32] A.B. Nowakowski, W.J. Wobig, D.H. Petering, Native SDS-PAGE: high resolution electrophoretic separation of proteins with retention of native properties including bound metal ions, Metallomics. 6(5) (2014) 1068-78. https://doi.org/10.1039/c4mt00033a.

[33] J. Xiao, S. Feng, X. Wang, et al., Identification of exosome-like nanoparticle-derived microRNAs from 11 edible fruits and vegetables, PeerJ. 6(2018) e5186. https://doi.org/10.7717/peerj.5186.

[34] K.M. Tembo, X. Wang, M. Bolideei, et al., Exploring the bioactivity of MicroRNAs Originated from Plant-derived Exosome-like Nanoparticles (PELNs): current perspectives, Journal of Nanobiotechnology. 23(1) (2025). https://doi.org/10.1186/s12951-025-03602-9.

[35] Y. Leng, L. Yang, S. Pan, et al., Characterization of blueberry exosome-like nanoparticles and miRNAs with potential cross-kingdom human gene targets, Food Science and Human Wellness. 13(2) (2024) 869-78. https://doi.org/10.26599/fshw.2022.9250074.

[36] Q. Zhang, J. Liu, H. Duan, et al., Activation of Nrf2/HO-1 signaling: An important molecular mechanism of herbal medicine in the treatment of atherosclerosis via the protection of vascular endothelial cells from oxidative stress, Journal of Advanced Research. 34(2021) 43-63. https://doi.org/10.1016/j.jare.2021.06.023.

[37] P. Mukhopadhyay, X. Lin, D. Bai, et al., Curcumin attenuates oxidative stress in RAW264.7 cells by increasing the activity of antioxidant enzymes and activating the Nrf2-Keap1 pathway, Plos One. 14(5) (2019). https://doi.org/10.1371/journal.pone.0216711.

[38] D. Zhao, X. Xia, M. Wei, et al., Overexpression of herbaceous peony miR156e-3p improves anthocyanin accumulation in transgenic Arabidopsis thaliana lateral branches, 3 Biotech. 7(6) (2017). https://doi.org/10.1007/s13205-017-1011-3.

[39] M.J. Kruger, N. Davies, K.H. Myburgh, et al., Proanthocyanidins, anthocyanins and cardiovascular diseases, Food Research International. 59(2014) 41-52. https://doi.org/10.1016/j.foodres.2014.01.046.

[40] J. Shi, Q. Jiang, S. Zhang, et al., MIR390 Is Involved in Regulating Anthracnose Resistance in Apple, Plants. 11(23) (2022). https://doi.org/10.3390/plants11233299.

[41] X. Zhao, F. Li, Y. Ji, et al., MiR9474-5p regulatory function in tomato fruit development and ripening: Comprehensive transcriptomic analysis, Postharvest Biology and Technology. 226(2025). https://doi.org/10.1016/j.postharvbio.2025.113558.

[42] S. Gupta, Y. Dong, P.P. Dijkwel, et al., Genome-Wide Analysis of ROS Antioxidant Genes in Resurrection Species Suggest an Involvement of Distinct ROS Detoxification Systems during Desiccation, International Journal of Molecular Sciences. 20(12) (2019). https://doi.org/10.3390/ijms20123101.

[43] A.A.A. Abdo, Y. Hou, F.A. Hassan, et al., Antioxidant potential and protective effect of modified sea cucumber peptides against H_2O_2-induced oxidative damage in vitro HepG2 cells and in vivo zebrafish model, International Journal of Biological Macromolecules. 266(2024). https://doi.org/10.1016/j.ijbiomac.2024.131090.

[44] C.M. Sánchez-López, M.C. Manzaneque-López, P. Pérez-Bermúdez, et al., Characterization and bioactivity of extracellular vesicles isolated from pomegranate, Food & Function. 13(24) (2022) 12870-82. https://doi.org/10.1039/d2fo01806c.

[45] M. De Robertis, A. Sarra, V. D'Oria, et al., Blueberry-Derived Exosome-Like Nanoparticles Counter the Response to TNF-α-Induced Change on Gene Expression in EA.hy926 Cells, Biomolecules. 10(5) (2020). https://doi.org/10.3390/biom10050742.

[46] K. Jomova, S.Y. Alomar, S.H. Alwasel, et al., Several lines of antioxidant defense against oxidative stress: antioxidant enzymes, nanomaterials with multiple enzyme-mimicking activities, and low-molecular-weight antioxidants, Archives of Toxicology. 98(5) (2024) 1323-67. https://doi.org/10.1007/s00204-024-03696-4.

[47] J. Wang, C. Hu, X. Ma, et al., The role of oxidative stress biomarkers in the development of peri-implant disease: A systematic review and meta-analysis, Journal of Dentistry. 146(2024) 105026. https://doi.org/10.1016/j.jdent.2024.105026.

[48] D. Tsikas, Assessment of lipid peroxidation by measuring malondialdehyde (MDA) and relatives in biological samples: Analytical and biological challenges, Analytical Biochemistry. 524(2017) 13-30. https://doi.org/10.1016/j.ab.2016.10.021.

[49] S. Li, S. Ma, P. Wang, et al., Flos Puerariae-derived exosomes-like nanoparticles ameliorate alcoholic liver disease by targeting IL-11-related signaling pathways and reactive oxygen species, Chemical Engineering Journal. 512(2025) 161896. https://doi.org/10.1016/j.cej.2025.161896.

[50] Z. Sun, Y. Zheng, T. Wang, et al., Aloe Vera Gel and Rind-Derived Nanoparticles Mitigate Skin Photoaging via Activation of Nrf2/ARE Pathway, International Journal of Nanomedicine. Volume 20(2025) 4051-67. https://doi.org/10.2147/ijn.S510352.

[51] A. Valentino, R. Conte, D. Bousta, et al., Extracellular Vesicles Derived from Opuntia ficus-indica Fruit (OFI-EVs) Speed Up the Normal Wound Healing Processes by Modulating Cellular Responses, International Journal of Molecular Sciences. 25(13) (2024) 7103. https://doi.org/10.3390/ijms25137103.

[52] J. Zhou, M. Guo, Y. Peng, et al., -derived exosome-like nanovesicles mitigate photoaging by attenuating oxidative stress and promoting collagen biosynthesis, Colloids and Surfaces B: Biointerfaces. 261(2026). https://doi.org/10.1016/j.colsurfb.2025.115412.